Impact of turbulence on flame brush development of acoustically excited rod-stabilized flames

Ashwini Karmarkar and Jacqueline O'Connor*

Department of Mechanical Engineering, Pennsylvania State University, University Park, PA 16802

Abstract

Coherent structures, such as those arising from hydrodynamic instabilities or excited by thermoacoustic oscillations, can significantly impact flame structure and, consequently, the nature of heat release. The focus of this work is to study how coherent oscillations of varying amplitudes can impact the growth of the flame brush in a bluff-body stabilized flame and how this impact is influenced by the free stream turbulence intensity of the flow approaching the bluff body. We do this by providing external acoustic excitation at the natural frequency of vortex shedding to simulate a highly-coupled thermoacoustic instability, and we vary the in-flow turbulence intensity using perforated plates upstream of the flame. We use high-speed stereoscopic particle image velocimetry to obtain the three-component velocity field and we use the Mie-scattering images to quantify the behavior of the flame edge. Our results show that in the low-turbulence conditions, presence of high-amplitude acoustic excitation can cause the flame brush to exhibit a step-function growth, indicating that the presence of strong vortical structures close to the flame can suppress flame brush growth. This impact is strongly dependent on the in-flow turbulence intensity and the flame brush development in conditions with higher levels of in-flow turbulence are minimally impacted by increasing amplitudes of acoustic excitation. These findings suggest that the sensitivity of the flow and flame to high-amplitude coherent oscillations is a strong function of the in-flow turbulence intensity.

Keywords: Turbulent flames; Turbulent flame brush; Hydrodynamic instability

1. Introduction

Large-scale coherent oscillations in a combustor flow field can significantly impact the stability and response of turbulent flames. In gas turbine combustors, coherent oscillations in the flow can drive fluctuations in the rate of heat release, which can couple with the resonant acoustic modes of the combustor and cause combustion instability [1]. Combustion instability can limit the operability of the engine and, in severe cases, damage engine hardware. As such, understanding the response of flames to coherent perturbations in the flow field is critically important for combustor design and implementation of instability mitigation techniques [2, 3].

Coherent oscillations can be a consequence of naturally occurring instabilities in the flow field or response of the flow to external perturbations, both of which typically manifest as coherent vortex shedding. Large-scale vortices can interact with flames, creating wrinkles in the flame front that lead to coherent and periodic fluctuations in the rate of heat release [4]. The flame response to a vortical disturbance can depend on the size and rotational strength of the vortex [5, 6]. The response is also impacted by several flame parameters, including the density ratio, Lewis Number, and degree of co-location between the flame and the shear layer in which the vortex is formed [7, 8]. In acoustically excited flows, the flame response is also a function of the amplitude and frequency of excitation [7, 9] and is governed by two competing effects: the evolution of the coherent vortices as they propagate along the flame and the dynamics of the flame, particularly the kinematic restoration effect created by flame propagation normal to itself [10]. In the near-field region, flame response grows linearly as the vortex grows and sheds, causing an increasingly large flame wrinkle. Further downstream, nonlinear behaviors dominate as the flame response decays due to kinematic restoration. This flame behavior can be significantly impacted by the presence of turbulence as a "de-correlating" force on the coherence flame wrinkling [11, 12].

Given that the coherent shedding of vortical structures can significantly impact the flame, it is important to characterize how the coherence of these structures and the coherent wrinkling on the flame generated by coherent structures are impacted by stochastic variations in the flow field arising from in-flow turbulence. The interaction between stochastic and coherent fluctuations is inherently complex since it is a dynamic interaction between processes at different scales. In non-reacting studies of bluff body wakes, increasing free-stream turbulence intensity accelerates the breakdown of vortices, thereby disrupting their coherence [13]. Additionally, increasing free-stream turbulence intensity can decrease the formation length of vortices, which can shorten the spatially developing shear layers and promote the merging of the shear layers into a fully turbulent jet [13, 14].

In reacting studies, this interaction is further complicated by the presence of a flame, as the free-stream turbulence not only impacts the coherent structures in the flow, but also the structure and propagation of the flame itself [15, 16]. In the absence of coherent structures, increasing inflow turbulence intensity causes increased flame wrinkling and faster development of the flame brush. The flame brush thickness of a turbulent flame is a measure of the time-averaged spatial extent of the flame location that arises from instantaneous motion of the flame front [17, 18]. The flame brush thickness and its development with downstream distance depends on in-flow turbulence intensity ($u'/\bar{u}$), the integral length scale, flame speed, and flame stretch sensitivity [17, 19, 20]. Experimental results from Kheirkhah et al. [19] show, using Mie-scattering images of a bluff-body stabilized flame, that increasing in-flow turbulence intensity can cause the flame front to become wrinkled, increasing the flame brush thickness. On an instantaneous basis, higher turbulence intensities lead to more frequent formation of cusps and holes in the flame. Chowdhury and Cetegen [21] also showed that increasing turbulence intensity increases the flame brush thickness in bluff-body stabilized flames, but the brush thickness saturates beyond 24%; it is suggested that this is potentially due to the prevalence of merging and extinction events in high-turbulence conditions.

As in non-reacting flows, turbulence and coherent motions interact in reacting flows to change the behavior of the flame. The present study focuses on understanding how stochastic and coherent fluctuations in the flow can impact the development of the flame brush in a rod-stabilized flame. It has been shown that the presence of in-flow turbulent fluctuations can disrupt the coherence of vortex shedding from a bluff-body and can cause variations in the cycle-to-cycle locations of the vortex cores and the flame location, known as 'phase jitter' [22]. Work by Hemchandra et al. [23] showed that acoustic forcing could impact the turbulent flame speed of harmonically-forced flames due to the interaction between the coherent and turbulent wrinkles on the flame, leading to faster wrinkle destruction with increasing distance from the flame stabilization point. The relative importance of this effect is dependent on the length scale of the coherent disturbance relative to the governing turbulent flame wrinkling scales, where forcing at coherent length scales close to the turbulent flame wrinkling scales accelerates turbulent flame propagation. Finally, Thumuluru [24] showed that the development of the flame brush in an acoustically-excited Bunsen flame is suppressed in the presence of high-amplitude acoustic excitation. The results showed that, in the presence of acoustic excitation, the flame brush growth exhibits a step-function development and this trend was observed over varying frequencies and fuel-types. These studies demonstrate that the presence of large-scale coherent oscillations in the flow field can fundamentally change the flame response of a turbulent premixed flame.

Put together, previous studies show that variations

in the flow – both stochastic and coherent – can significantly impact the stability and dynamics of the flame. The goal of this work is to characterize the impact of external acoustic forcing on the development of the turbulent flame brush for varying levels of in-flow turbulence by considering the impact of turbulence on both the coherent oscillations in the flow and the flame. Our results show that in low-turbulence intensity conditions, the development of the flame brush is suppressed in the presence of vortices, as in the work by Thumuluru [24]. However, as the in-flow turbulence intensity is increased, the development of the flame brush is minimally impacted by the acoustic excitation for the same ratio of acoustic forcing perturbation to turbulence intensity.

2. Methods

2.1. Experimental facility

The experimental facility is a modified version of that used by Tyagi et al. [25] and only a brief overview is provided here. The flame is a rod-stabilized V-flame in an unconfined configuration. Upstream of the flame, the burner consists of a 30 mm $\times$ 100 mm burner exit with a 100 mm long, 3.18 mm diameter rod that runs along the center of the burner, as shown in Fig. 1. Premixed air and fuel (natural gas) at stoichiometric conditions enter through the base of the burner and pass through two ceramic honeycomb flow-straighteners; perforated plates are used for turbulence generation. The turbulence generation plates have a staggered hole pattern with 3.2 mm hole diameters and a 40% open area. Two perforated plates located 10 mm and 30 mm upstream of the burner exit are used for the high in-flow turbulence intensity (11%) conditions and no perforated plates are used for low in-flow turbulence intensity (5%) conditions. The bulk flow velocity is held constant at 10 m/s in all conditions. External acoustic excitation is added using a speaker at the base of the burner, upstream of both honeycombs, as shown in Fig. 1. The input to the speaker is an amplified sinusoidal signal generated by a function generator. The frequency of the input signal is set to 580 Hz, which is close to the characteristic frequency of vortex shedding; the natural vortex-shedding frequency was measured in a previous study [26]. The amplitude of acoustic excitation is varied by adjusting the peak-to-peak voltage (V_{pp}) of the input signal.

2.2. Diagnostics

Stereoscopic particle image velocimetry (PIV) is performed at 10 kHz with a dual cavity, Nd:YAG laser (Quantronix Hawk Duo) operating at 532 nm in forward-forward scatter mode. A 50 mm tall laser sheet is created using a combination of mirrors and three cylindrical lenses; the angle between the laser sheet and each camera sensor (Photron FASTCAM SA5) is about 35 degrees. Each camera is equipped with a 100 mm f/2.8 lens (Tokina Macro) and a Nikon tele-converter to allow for a safe stand-off distance

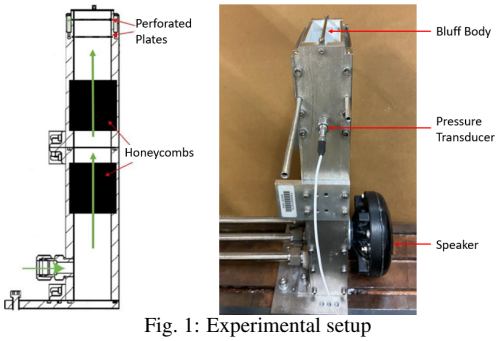

Fig. 1: Experimental setup

between the sensor and the burner. This setup has a 32 mm $\times$ 53 mm field of view and images are collected at 10 kHz in double-frame mode with a pulse separation of 14 μs. Aluminum oxide particles of diameters 0.5-2.0 μm are used for seeding. To reduce flame luminosity in the images, near-infrared filters (Schneider Kreuznach IR MTD) and laser line filters (Edmund Optics TECHSPEC 532 nm CWL) are used on each camera.

LaVision's DaVis 8.3 is used to perform vector calculations from Mie scattering images. These calculations include a multi-pass algorithm with varying window sizes ranging from 64 $\times$ 64 to 16 $\times$ 16 and a 50% overlap. This processing results in a vector spacing of 0.48 mm/vector. A universal outlier detection scheme, with a 3$\times$ median filter, is used for post-processing of the vector fields. The instantaneous uncertainties in the vector fields range from $1.5 - 2.8\ m/s$ in the reacting conditions and $0.7 - 2.1\ m/s$ in the non-reacting cases, using the uncertainty calculation feature in Davis. The uncertainties in the RMS magnitude of the vector fields range from $0.03 - 0.05\ m/s$ in all cases; most analysis in this paper relies on RMS values. A total of 5000 vector fields are obtained for each condition.

The Mie-scattering images from PIV are also used to identify the flame location. The process for binarization and edge detection in the Mie-scattering images includes five steps. First, images are Gaussian filtered for blurring sharp gradients due to noise. Second, median filtering with a window size of 10 pixels $\times$ 10 pixels is applied to remove the effect of salt and pepper noise due to scattering from aluminum oxide particles. Next, a smoothing operation is performed using bilateral filtering, and then Otsu's method is applied on the smoothed image from and multi-level thresholding is used to account for the spatial variation in signal intensity; the number of thresholds is varied between 4 and 8 depending on the conditions. Finally, the minimum threshold value is used to binarize the processed image into a value of 0 in the reactants and 1 in the products. These binarized images are used to calculate the time-averaged and phase-averaged progress variable contour, $\bar{c}$.

The phase-averaged progress variable contours are

computed by averaging binarized images at each phase, where each phase has 290 images. Since the the frequency of acoustic forcing, $f_0 = 580\ Hz$, is not an integer multiple of the sampling frequency ($f_s = 10\ kHz$), we interpolate between images to obtain multiple images at a single phase. To do this interpolation, we use a non-rigid image registration algorithm to compute the flame location at the appropriate time between one image and the next. The non-rigid image registration method uses the `imregdemons` function in MATLAB and calculates a displacement field from one image to the next that can then be scaled to determine the intermediary flame location. This method was previously used in our group by Tyagi et al. [25]; this reference contains a more detailed discussion of the method and the supplementary material includes a thorough sensitivity and uncertainty analysis associated with non-rigid image registration.

2.3. Test Matrix

This study considers the impact of both turbulence intensity and coherent fluctuation intensity on flame brush development. The acoustic energy input was varied by adjusting the peak-to-peak voltage amplitude (V_{pp}) of the sinusoidal wave input to the speaker and the magnitude of stochastic fluctuations was varied using the perforated plates. We consider six acoustic amplitudes and two turbulence conditions.

In order to individually characterize the stochastic and coherent fluctuation magnitudes, we perform a *triple decomposition* on the velocity field [27].

$$u(x,y,t) = \bar{u}(x,y) + \tilde{u}(x,y,t) + u'(x,y,t)$$

Here, $u(x,y,t)$ is the time-varying velocity signal at any spatial location in the flow; $\bar{u}(x,y)$ is the time-averaged velocity at the given location, assuming the signal is statistically stationary; $\tilde{u}(x,y,t)$ is the coherent component of the velocity signal, extracted by performing a frequency domain filtering of the signal around the frequency of excitation; and $u'(x,y,t)$ is the stochastic content in the velocity signal. This stochastic component is computed by reconstructing the fluctuating velocity signal *without* the content at the forcing frequency and its harmonics. In these data, the amplitude of the velocity fluctuation at the first harmonic is nearly two orders of magnitude lower than the response at the forcing frequency; as such, we do not expect it to significantly impact the coherent dynamics in the flow field. However, we remove this component when computing the stochastic components of the fluctuating velocity field to avoid any coherent content.

Figure 2 shows the variations in stochastic ($u'_{in}/\bar{u}_{in}$) and harmonic ($\tilde{u}_{in}/\bar{u}_{in}$) velocity components with varying excitation amplitude and plate condition. These "input" parameters are determined using velocity data obtained from PIV measurements of non-reacting flow through the burner without the

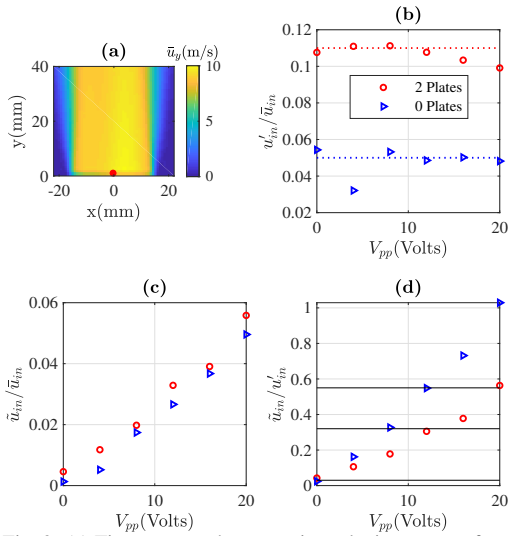

Fig. 2: (a) Time-averaged streamwise velocity contour for a representative condition; red dot marks the location where the velocity signal is extracted, (b) RMS magnitude of the stochastic component of velocity, (c) RMS magnitude of the coherent component of velocity, and (d) Ratio of coherent-to-stochastic RMS magnitudes.

bluff body. The calculation is made along the burner centerline at a location close to the burner exit, indicated by the red dot in Fig. 2(a), which shows a contour plot of the time-averaged streamwise velocity for a single condition. The instantaneous velocity is averaged over a 3×3 window to avoid spurious results from single-point measurements. The Reynolds number based on bluff-body diameter is held constant for both plate conditions, $Re_D = 2036$. In the condition with both plates in, the turbulent Reynolds number, computed using the integral length scale ($l_0 \approx 2mm$) is, $Re_T = 140$; the turbulent Reynolds number at the low-turbulence condition is not well-defined given the low value of turbulence intensity.

The in-flow turbulence intensity, ($u'_{in}/\bar{u}_{in}$), shown in Fig. 2(b), is generally constant with excitation amplitude, indicating that the energy added by the acoustic forcing is predominantly coherent, as would be expected. The high-turbulence condition (two plates) has a turbulence intensity of around 11% and the low-turbulence condition (no plates) has a turbulence intensity of 5%. The RMS amplitude of the coherent oscillation, ($\tilde{u}_{in}/\bar{u}_{in}$), shown in Fig. 2(c), varies linearly with excitation amplitude and is independent of the turbulence intensity. Finally, Fig. 2(d) shows the relative contributions of the coherent and stochastic components, ($\tilde{u}_{in}/u'_{in}$), for both turbulence conditions. Comparable ratios of these input parameters for both turbulence intensities can be seen at $\tilde{u}_{in}/u'_{in} \approx 0\%$ (no-forcing condition), 32%, and 55%, as indicated by horizontal black lines in the plot. (At the condition with no excitation ($V_{pp} = 0V$), the coherent content is non-zero because turbulent oscilla-

tions in the flow field manifest themselves at a spectrally broad range of scales; as such, it is expected that there will be some fluctuation content at the frequency of excitation even in the absence of external excitation. However, since the magnitude of this content is sufficiently small, we can refer to this condition as $\tilde{u}_{in}/u'_{in} \approx 0\%$). We focus our analysis of the flame brush development at these three conditions to understand the role of turbulence intensity in governing coherent response and the flame brush development.

3. Results

3.1. Coherent vortical response characterization

Figure 2 shows the variation in the coherent and stochastic flow components with varying degrees of acoustic excitation in the incoming flow. In order to understand how the input conditions impact the coherence of the vortices shed from the bluff body, we perform a triple decomposition on the flow in the shear layer in both non-reacting and reacting flow with the bluff body in place. Figure 3 (left), shows a contour plot of the time-averaged vorticity for a single non-reacting condition. To characterize the shear layer response, we calculate stochastic and coherent velocity statistics using the mean of a 3×3 window centered at the location of the maximum time-averaged vorticity for each case, depicted by the black circle. Figure 3 (right) shows the variation in the coherent shear layer response ($\tilde{u}_{sl,r}$) relative to stochastic fluctuations in the shear layer ($u'_{sl,r}$) versus the ratio of coherent-to-stochastic oscillations in the in-flow ($\tilde{u}_{in}/u'_{in}$) for both turbulence conditions for reacting and non-reacting flow.

The three conditions with comparable input amplitudes, $\tilde{u}_{in}/u'_{in} \approx 0\%, 32\%$, and 55%, are marked by the solid black lines. For the same excitation input, the coherent response relative to the stochastic fluctuations is significantly higher in the low-turbulence conditions as compared to the high-turbulence conditions. The higher level of coherent oscillation relative to stochastic oscillation in the non-reacting cases indicates that increasing turbulence intensity modulates the flow field and reduces the coherence of the vortices in the shear layer. The fact that this loss of coherence is present in both non-reacting and reacting conditions is evidence that this behavior is not a result of expansion by the flame; this finding is consistent with results reported in the literature [13].

3.2. Time-averaged flow and flame profiles

Figure 4 shows the time-averaged vorticity contours for the three reacting-flow conditions with comparable coherent-to-stochastic input amplitudes. The black solid lines represent the mean flame edge, obtained by extracting the progress variable $\bar{c} = 0.5$ contour from the time-averaged binarized Mie-scattering images. The dotted black lines depict the $\bar{c} = 0.3$ and $\bar{c} = 0.7$ contours and are provided to

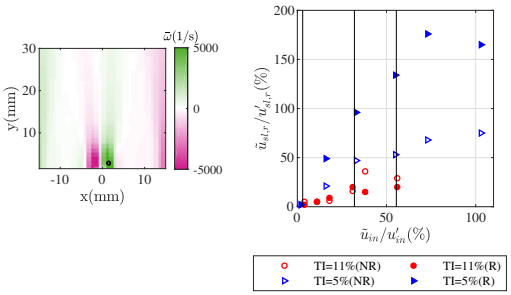

Fig. 3: Coherent velocity response in the shear layer as a function of in-flow forcing input for both turbulence conditions for reacting (R) and non-reacting (NR) flows.

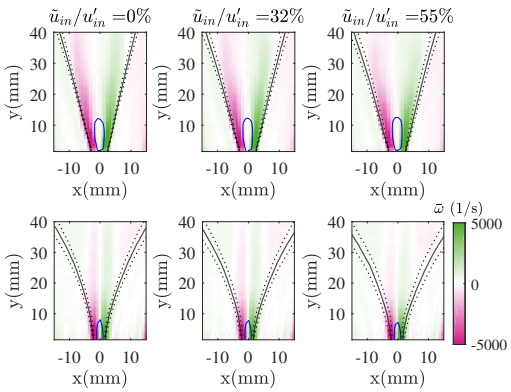

Fig. 4: Time-averaged vorticity contours for the low-turbulence (top row) and high-turbulence (bottom row) conditions. The black solid line depicts the $\bar{c} = 0.5$ contour and the dotted lines represent the $\bar{c} = 0.3$ and $\bar{c} = 0.7$ contours. The blue contour represents the limits of recirculation zone, $\bar{u}_y = 0$.

illustrate the extent of the flame brush. The blue contour in the center is the $\bar{u}_y = 0$ contour, representing the limits of the recirculation zone in the wake of the bluff body that acts to stabilize the flame.

In the low-turbulence conditions (top row), $TI = 5\%$, increasing the input coherent excitation causes a marginal increase in the mean flame angle relative to the central axis and in the flame brush thickness. Both increases are likely a consequence of the fluctuations in the flame edge caused by coherent wrinkling due to interaction with vortices. Compared to the low-turbulence conditions, the conditions with the higher levels of in-flow turbulence (bottom row), $TI = 11\%$ show faster downstream decay of time-averaged vorticity. Further, the recirculation zone, depicted by the blue contour in Fig. 4, is shorter in the high-turbulence case than in the low-turbulence case, which has been attributed to the shorter vortex formation length in the high-turbulence conditions [13]. The higher levels of in-flow turbulence intensity increase the turbulent flame speed, s_T, causing a wider flame angle. The mean flame brush is also wider in the conditions with higher levels of free-stream tur-

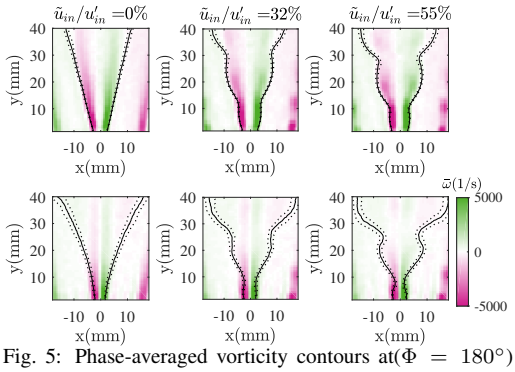

Fig. 5: Phase-averaged vorticity contours at($\Phi = 180°$) phase for the $TI = 5\%$ (top row) and the $TI = 11\%$ (bottom row) conditions. The solid black lines depict the phase-averaged $\bar{c} = 0.5$ contour and the dotted lines represent the phase-averaged $\bar{c} = 0.3$ and $\bar{c} = 0.7$ contours. (Videos of these conditions are available in the supplementary material.)

bulence, which is also consistent with previous studies [19, 21]. Using a linear curve fit of the flame edge to compute a flame angle, the flame stabilization angle, Θ, increases from $13°$ to $21°$ between the low- and the high-turbulence conditions in the absence of external excitation. This increase indicates that the increasing turbulence intensity causes the flame speed, which is proportional to $\sin(\Theta)$, to increase by a factor of 1.6. Finally, comparing the time-averaged contours across varying excitation amplitudes, the time-averaged vorticity contours and flame edges in the high-turbulence conditions are only marginally impacted by the increasing coherent excitation amplitude.

3.3. Phase-averaged flow profiles

The time-averaged flame edge and vorticity contours shown in Fig. 4 illustrate the differences in the mean flow and flame between the low- and high-turbulence conditions. However, a phase-average of the results must be used to understand how coherent forcing impacts development of the flame brush. Figure 5 shows the phase-averaged vorticity contours at a single phase for three coherent forcing conditions and both turbulence intensities. The black solid lines depict the phase-averaged $\bar{c} = 0.5$ contour and the black dotted lines depict the phase-averaged $\bar{c} = 0.3$ and $\bar{c} = 0.7$ contours.

The phase-averaged contours in Fig. 5 and videos in the supplementary material show that, for both turbulence conditions, increasing coherent excitation amplitude causes increasingly large flame front wrinkles. In the condition with no acoustic forcing at both turbulence intensities, concentrated regions of vorticity form in the shear layer but they do not exhibit any spatial coherence and the flame contour in this condition moves randomly with the turbulent field. In the low turbulence conditions with acoustic forcing, tightly concentrated regions of vorticity form at the bluff body and decay as they travel downstream. Wrinkles in the flame edge are closely coupled with the coherent shedding of vortical structures. For example, the formation of flame cusps can be seen at $y = 10\ mm$ and at $y = 27\ mm$, and these cusps line up with the boundaries of the vortices. The videos of phase-averaged vorticity for the conditions shown in Fig. 5, provided in the supplementary material, show that at the low-turbulence conditions, the wrinkling of the flame edge closely tracks the location of each vortex and the flame edges wrap around the shed vortices at all phases. The videos further illustrate that, in the conditions with low turbulence intensity, the flame structure is strongly impacted by the oscillations in the flow.

In the high-turbulence conditions with acoustic forcing, the vortical structures are weaker, as quantified in Fig. 3, and the vorticity magnitude decays rapidly downstream as a result of the interaction between turbulence and the vortices. The flame wrinkles, however, persist even as the vortices decay. The curvature of the flame wrinkles is weaker, as evidenced by the larger radius of curvature at the cusps of the flame at $y = 8\ mm$ and $y = 26\ mm$. There are two contributing factors to these behaviors. First, since the vortices are weaker, the resulting strain on the flame is lower. At the same time, however, the turbulent flame speed is higher, which enhances the kinematic restoration effect and smooths flame wrinkles on a shorter timescale [12]. The phase-averaged videos for the high-turbulence conditions, provided with the supplementary material, show that as acoustic excitation amplitude is increased, the flame edge exhibits stronger coherent oscillations. However, unlike the low-turbulence conditions, the flame edge wrinkling in the high-turbulence conditions does not closely track the vortices; this effect is amplified with downstream distance. This is likely a consequence of the increased turbulent flame speed, s_T, causing both fast wrinkle smoothing and allowing the flame to propagate further upstream in the flow and away from the shear layer, reducing the direct interaction between the vortices and the flame.

3.4. Phase-averaged turbulent flame brush development

The phase-averaged results in Fig. 5 show that the conditions with higher turbulence intensities have a wider flame brush, as depicted by the dotted lines representing the $\bar{c} = 0.3$ and the $\bar{c} = 0.7$ contours. In order to quantitatively characterize the relative impact of stochastic and coherent fluctuations on flame-brush development, we calculate the turbulent flame brush thickness along the phase-averaged $\bar{c} = 0.5$ contour by calculating the distance between the $\bar{c} = 0.3$ contour and the $\bar{c} = 0.7$ contour along the normal from the $\bar{c} = 0.5$ contour.

Figure 6 depicts the variation in the phase-averaged flame brush thickness, δt_f, along the phase-averaged $\bar{c} = 0.5$ contour, l_f. The plots of flame brush development in Fig. 6 correspond directly to the phase

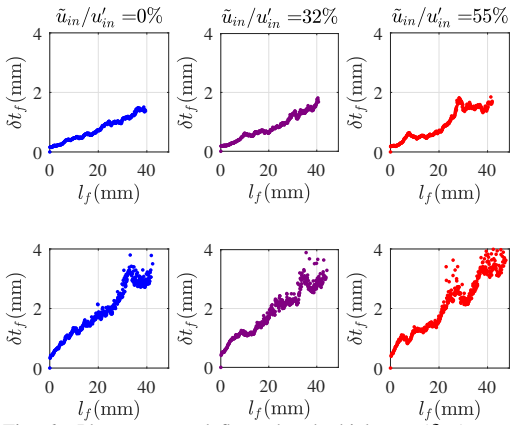

Fig. 6: Phase-averaged flame brush thickness (δt_f) as a function of the flame coordinate (l_f) for the $TI = 5\%$ (top row) and the $TI = 11\%$ (bottom row) conditions for comparable acoustic input conditions at ($\Phi = 180°$)

.

averages shown in Fig. 5 at ($\Phi = 180°$). There is a significant difference in the development of the flame brush between the low-turbulence (top row) and the high-turbulence (bottom row) conditions. For the low-turbulence conditions, the flame brush thickness linearly increases along the flame edge in the absence of acoustic forcing, consistent with the findings in the literature [17]. However, as the excitation amplitude increases, the flame brush development exhibits a step-function behavior. The flame brush thickness increases sharply at the location of the flame cusp and the brush growth is subsequently suppressed until the next cusp is encountered. A similar result was reported by Thumuluru [24] for an acoustically-forced Bunsen flame. This suppression of flame brush development was attributed to the fact that the coherent excitation modulates the turbulence field and, consequently, the local consumption speed. In the same study, it was also observed that flame stretch effects do not have a dominant effect on this development, as the flame brush development was insensitive to different fuel mixtures with varying stretch sensitivities.

At the high-turbulence conditions, the flame brush grows faster with downstream distance, which is a result of increased turbulent wrinkling of the flame. Unlike the low-turbulence conditions, the flame brush development in the high-turbulence conditions is largely independent of the coherent excitation amplitude. The flame brush growth in the high-turbulence conditions is largely monotonic, although small peaks can be seen further downstream at random intervals; these peaks do not correspond to any phase-averaged flame features and are likely a consequence of increased small-scale wrinkles and pocket formation. The rate of flame brush growth in the high-turbulence conditions is similar across all excitation amplitudes and phases, indicating that this development is minimally impacted by the presence of coherent excitation. There are two contributing factors to this behavior. First, the increased turbulence intensity disrupts the coherence of the vortical structures, which in turn causes the coherent flame edge to be more weakly wrinkled. Second, with increased levels of in-flow turbulence intensity, the flame brush development is predominantly governed by turbulent diffusion effects and is hence not substantially impacted by the coherent excitation. In this case, it is unlikely that the turbulent flame speed is significantly modulated by coherent forcing, as was suggested by Hemchandra et al. [23], since the integral length scale of the turbulence (∼2 mm) is approximately an order of magnitude shorter than the convective length scale of the coherent disturbances (∼20 mm).

Figure 7 further illustrates the sensitivity of the phase-averaged flame-brush development to in-flow turbulence intensity. The plots in Fig. 7 depict the flame brush development at four phases for the highest amplitude forcing conditions, $\tilde{u}_{in}/u'_{in} = 55\%$. The blue curves depict the phase-averaged $\bar{c} = 0.5$ contour, and the orange scatter plots depict the phase-averaged flame brush thickness. The low-turbulence conditions show that the flame brush thickness increases sharply at the location of the flame cusp and the brush development is suppressed until the next cusp; this pattern is repeated at each phase. In the high-turbulence conditions, however, the flame brush development is minimally impacted by the location of the flame wrinkles across all phases.

4. Conclusions

This study characterizes the relative impact of coherent excitation and in-flow turbulence intensity on the development of the turbulent flame brush thickness in a rod-stabilized flame at stoichiometric conditions. We study two in-flow turbulence conditions, $TI = 5\%$ and 11%, along with six excitation amplitudes for each condition. We characterize the input to the flame using non-reacting free-stream measurements taken close to the burner exit and match the ratio of coherent-to-stochastic fluctuation amplitudes for both turbulence conditions. We characterize the shear layer response with the bluff body using the signal at the maximum time-averaged vorticity location. Our results show that for the same relative input of coherent excitation, the low-turbulence condition has a higher coherent vortical response compared to the high-turbulence condition, as higher levels of in-flow turbulence disrupt the coherence of vortices.

The reacting flow results show that the flame wrinkling is coupled with the strength of the vortices; the flame edges in conditions with the higher levels of in-flow turbulence are weakly wrinkled as compared to the flame edges in conditions with low levels of in-flow turbulence. The phase-averaged flame brush thickness development is highly dependent on in-flow turbulence intensity. The flame brush growth exhibits a step-function like behavior along the flame edge with steps that corresponds to the cusping of the flame

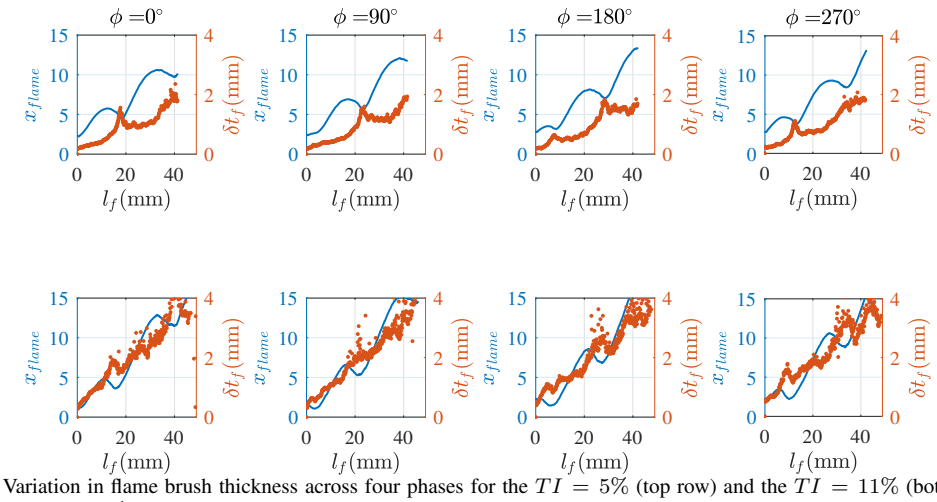

Fig. 7: Variation in flame brush thickness across four phases for the $TI = 5\%$ (top row) and the $TI = 11\%$ (bottom row) conditions for $\tilde{u}_{in}/u'_{in} = 55\%$. The blue curves depict the corresponding phase-averaged $\bar{c} = 0.5$ contours.

at low in-flow turbulence levels, but the flame brush development is relatively insensitive to acoustic forcing at the high in-flow turbulence conditions. This result is significant because it quantitatively demonstrates that the sensitivity of the flame response to coherent excitation is a function of the in-flow turbulence intensity. We see that flows with higher levels of in-flow turbulence respond less severely to external acoustic excitation for two reasons. First, the higher levels of turbulence weaken the coherence of vortices shed from acoustic excitation. Second, the higher turbulent flame speed destroys coherent flame wrinkles on a shorter timescale. These results indicate that turbulence has a critical impact on multiple steps of the thermoacoustic coupling process, including both the flow field development as well as flame propagation.

Acknowledgments

This material is based upon work supported by the National Science Foundation under Grant CBET-1749679. Any opinions, findings, and conclusions or recommendations expressed in this material are those of the authors and do not necessarily reflect the views of the National Science Foundation.

References

[1] T. J. Poinsot, A. C. Trouve, D. P. Veynante, S. M. Candel, E. J. Esposito, Vortex-driven acoustically coupled combustion instabilities, Journal of Fluid Mechanics 177 (1987) 265–292.

[2] S. M. Candel, Combustion instabilities coupled by pressure waves and their active control, in: Symposium (International) on Combustion, Vol. 24, 1992, pp. 1277–1296.

[3] K. McManus, T. Poinsot, S. M. Candel, A review of active control of combustion instabilities, Progress in Energy and Combustion Science 19 (1) (1993) 1–29.

[4] P.-H. Renard, D. Thevenin, J.-C. Rolon, S. Candel, Dynamics of flame/vortex interactions, Progress in Energy and Combustion Science 26 (3) (2000) 225–282.

[5] T. Poinsot, D. Veynante, S. Candel, Quenching processes and premixed turbulent combustion diagrams, Journal of Fluid Mechanics 228 (1991) 561–606.

[6] C. J. Mueller, J. F. Driscoll, D. L. Reuss, M. C. Drake, M. E. Rosalik, Vorticity generation and attenuation as vortices convect through a premixed flame, Combustion and Flame 112 (3) (1998) 342–358.

[7] B. Emerson, T. Lieuwen, Dynamics of harmonically excited, reacting bluff body wakes near the global hydrodynamic stability boundary, Journal of Fluid Mechanics 779 (2015) 716–750.

[8] J.-M. Samaniego, T. Mantel, Fundamental mechanisms in premixed turbulent flame propagation via flame–vortex interactions: Part 1: Experiment, Combustion and Flame 118 (4) (1999) 537–556.

[9] A. Chaparro, E. Landry, B. M. Cetegen, Transfer function characteristics of bluff-body stabilized, conical v-shaped premixed turbulent propane–air flames, Combustion and Flame 145 (1-2) (2006) 290–299.

[10] S. Shanbhogue, D.-H. Shin, S. Hemchandra, D. Plaks, T. Lieuwen, Flame-sheet dynamics of bluff-body stabilized flames during longitudinal acoustic forcing, Proceedings of the Combustion Institute 32 (2) (2009) 1787–1794.

[11] S. Hemchandra, T. Lieuwen, Local consumption speed of turbulent premixed flames–an analysis of "memory effects", Combustion and Flame 157 (5) (2010) 955–965.

[12] L. J. Humphrey, B. Emerson, T. C. Lieuwen, Premixed turbulent flame speed in an oscillating disturbance field, Journal of Fluid Mechanics 835 (2018) 102–130.

[13] I. Khabbouchi, H. Fellouah, M. Ferchichi, M. S. Guellouz, Effects of free-stream turbulence and reynolds number on the separated shear layer from a circular cylinder, Journal of Wind Engineering and Industrial Aerodynamics 135 (2014) 46–56.

[14] M. Arie, M. Kiya, Y. Suzuki, M. Hagino, K. Takahashi, Characteristics of circular cylinders in turbulent

flows, Bulletin of JSME 24 (190) (1981) 640–647.
[15] J. F. Driscoll, Turbulent premixed combustion: Flamelet structure and its effect on turbulent burning velocities, Progress in Energy and Combustion Science 34 (1) (2008) 91–134.
[16] P. Clavin, Dynamic behavior of premixed flame fronts in laminar and turbulent flows, Progress in Energy and Combustion Science 11 (1) (1985) 1–59.
[17] A. Lipatnikov, J. Chomiak, Turbulent flame speed and thickness: phenomenology, evaluation, and application in multi-dimensional simulations, Progress in Energy and Combustion Science 28 (1) (2002) 1–74.
[18] N. Peters, Turbulent Combustion, Cambridge Monographs on Mechanics, Cambridge University Press, 2000.
[19] S. Kheirkhah, Ö. Gülder, Topology and brush thickness of turbulent premixed v-shaped flames, Flow, Turbulence, and Combustion 93 (3) (2014) 439–459.
[20] M. Namazian, I. Shepherd, L. Talbot, Characterization of the density fluctuations in turbulent v-shaped premixed flames, Combustion and Flame 64 (3) (1986) 299–308.
[21] B. R. Chowdhury, B. M. Cetegen, Experimental study of the effects of free stream turbulence on characteristics and flame structure of bluff-body stabilized conical lean premixed flames, Combustion and Flame 178 (2017) 311–328.
[22] S. J. Shanbhogue, M. Seelhorst, T. Lieuwen, Vortex phase-jitter in acoustically excited bluff body flames, International Journal of Spray and Combustion Dynamics 1 (3) (2009) 365–387.
[23] S. Hemchandra, N. Peters, T. Lieuwen, Heat release response of acoustically forced turbulent premixed flames—role of kinematic restoration, Proceedings of the Combustion Institute 33 (1) (2011) 1609–1617.
[24] S. K. Thumuluru, Effect of harmonic forcing on turbulent flame properties, Ph.D. thesis, Georgia Institute of Technology (2010).
[25] A. Tyagi, I. Boxx, S. Peluso, J. O'Connor, Statistics and topology of local flame–flame interactions in turbulent flames, Combustion and Flame 203 (2019) 92–104.
[26] A. Karmarkar, A. Tyagi, S. Hemchandra, J. O'Connor, Impact of turbulence on the coherent flame dynamics in a bluff-body stabilized flame, Proceedings of the Combustion Institute 38 (2) (2021) 3067–3075.
[27] A. F. Hussain, Coherent structures—reality and myth, Physics of Fluids 26 (10) (1983) 2816–2850.